Combining radiationless interference with evanescent field amplification

Varat Intaraprasonk,[1] Zongfu Yu,[2] and Shanhui Fan[2,*]

[1]*Department of Applied Physics, Stanford University, Stanford, California 94305, USA*
[2]*Department of Electrical Engineering, Stanford University, Stanford, California 94305, USA*
**Corresponding author: shanhui@stanford.edu*

Received January 15, 2010; revised March 27, 2010; accepted April 8, 2010;
posted April 16, 2010 (Doc. ID 122743); published May 7, 2010

The conventional approach for radiationless interference exploits the interference of evanescent components for the purpose of deep-subwavelength focusing and image formation. As a result, deep subwavelength feature size is achieved at the price of severe exponential decay of the field strength. We propose to overcome the limitation of the conventional approach by combining radiationless interference with evanescent field amplification as provided by the surface polaritons at the interface between positive- and negative-dielectric materials. Our approach removes the exponential decay and, moreover, allows a much wider range of wave vectors, including both propagating and evanescent field components, to participate in the image-formation process.

OCIS codes: 070.7345, 240.0240.

The capability for focusing and manipulating light at deep subwavelength scale is of fundamental interest in optical technology. Traditional techniques for light focusing are constrained by the fundamental limit of diffraction and cannot focus light into a spot that is far smaller than the wavelength. The goal of overcoming such diffraction limit has motivated many efforts in near-field optics, negative index metamaterials, and plasmonics [1–4]. As a recent development, the scheme of radiationless interference has generated substantial interest [5–15]. In this scheme [5], an appropriately specified field distribution on a source plane is used to generate a subwavelength focal spot some distance away, through the interference of the evanescent components in the source field [Fig. 1(a)]. This scheme has been demonstrated experimentally using microwave [8,9], and designs have been proposed to extend it to optical wavelengths [13].

One of the basic limitations of radiationless interference, however, lies in the substantial energy decay as the fields propagate from the source plane to the focal spot [Fig. 1(b)]. In this Letter, we propose to overcome such difficulty by combining radiationless interference with evanescent field amplification. The setup is shown in Fig. 1(c); the field is specified at the source plane at $z=0$ in order to form a focal spot at $z=d$. In the region $z>d$, the space is filled with material with a negative dielectric constant. The excitation of the surface polariton gives a large amplification for evanescent fields and can compensate for the evanescent decay from the free-space propagation [Fig. 1(d)].

In addition to overcoming exponential decay, introducing evanescent amplification also provides new opportunities. In the conventional radiationless interference scheme, one exclusively uses evanescent components, since there is a drastic difference in the propagation behaviors between the propagating and the evanescent Fourier components. In contrast, with the use of the evanescent amplification, the propagating and evanescent fields have similar behaviors. Therefore, both parts can be used for image formation purposes, resulting in better image quality.

As a starting point we briefly review the concept of radiationless interference in 2D in free space with a dielectric constant ϵ_d, where the field F is governed by

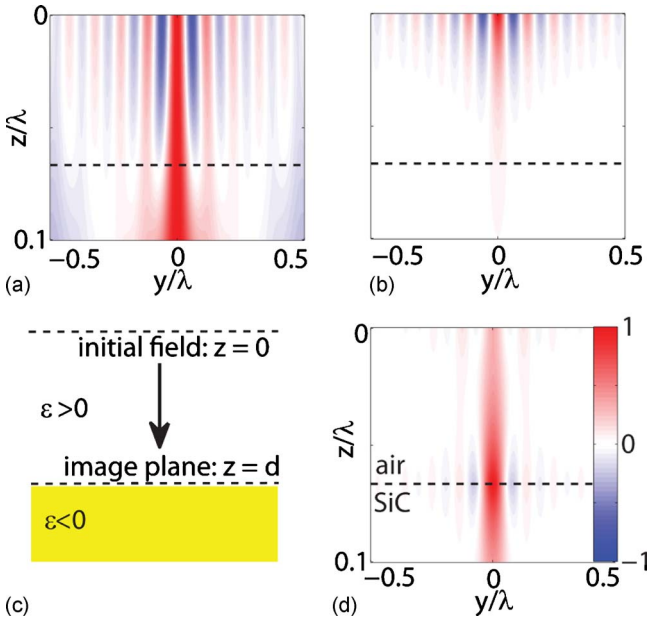

Fig. 1. (Color online) (a) Subwavelength focusing using initial field distribution following [5], $d=\lambda/15$, FWHM $=\lambda/18$. Following [5] the plot is generated such that each z plane has maximum amplitude of 1. (b) Same as (a) but in linear scale. The peak amplitude actually decays significantly (to 7.8% at focal point). (c) Schematic for the focusing with evanescent amplification. (d) Result of (c) in linear scale. The negative-permittivity material is SiC at $\lambda=10.56\ \mu$m with $\epsilon_m=-1.035+0.13i$. We achieve the same values of d and FWHM as (a) and (b) but get an amplitude gain of 3.

0146-9592/10/101659-3/$15.00

$$\left(\frac{\partial^2}{\partial y^2}+\frac{\partial^2}{\partial z^2}+k_d^2\right)F=0, \tag{1}$$

where $k_d^2=\epsilon_d(\omega/c)^2$, ω is the angular frequency, and c is the speed of light. For each Fourier component of the field F with parallel wavevector in the y direction k_y, its propagation in the z direction is given by

$$F(k_y,z)=F(k_y,z=0)T_f(k_y,z),$$

where

$$T_f(k_y,z)=\exp(ik_{z,d}(k_y)z). \tag{2}$$

Here, $k_{z,d}=+\sqrt{k_d^2-k_y^2}$. For high spatial frequencies $k_y \gg k_d$, $k_{z,d}\approx ik_y$,

$$T_f(k_y,z)\approx\exp(-k_yz). \tag{3}$$

For radiationless focusing, in order to produce a focal spot of size $l\approx 2\pi/q_0$ at $z=d$, one chooses a field distribution in the source plane such that fields in the wave-vector space $F(k_y)$ are centered around $k_y=q_0$ [5,15]. As a result, one can see from Eq. (3) that, upon reaching the focal point at $z=d$, the field intensity should have decayed by a factor of approximately $\exp(-2q_0d)=\exp(-4\pi d/l)$. (The exact factor of the amplitude decay, for on-axis field, in the case of a source field distribution as specified in [5], is $\exp(-q_0d)\sqrt{\pi/2}q_0d$.) Thus, while the radiationless focusing scheme allows the creation of a subwavelength focal spot, it does so at the price of substantial power decay, as shown in the plot of Fig. 1(b), where the field is plotted on a linear scale. The amount of power decay is 99.4%, even when one seeks to focus to a distance that is equal to the size of the focal spot.

Here we propose to overcome this limitation by combining the radiationless interference scheme with the evanescent field enhancement effect [1]. As a demonstration, we place a negative dielectric region with $\epsilon_m\approx-\epsilon_d$ at $z>d$ and consider the TM polarization by setting the field F to be the magnetic field along the x direction. The total field F_t at the image plane is then related to the incident field F_i at the source plane as

$$F_t(k_y,d)=F_i(k_y,0)T(k_y),$$

where

$$T(k_y)=(1+r(k_y))\exp(ik_{z,d}d). \tag{4}$$

Here

$$r(k_y)=\left(\frac{k_{z,d}}{\epsilon_d}-\frac{k_{z,m}}{\epsilon_m}\right)\Big/\left(\frac{k_{z,d}}{\epsilon_d}+\frac{k_{z,m}}{\epsilon_m}\right) \tag{5}$$

is the reflection coefficient from the interface. $k_{z,m}=+\sqrt{\epsilon_m(\omega/c)^2-k_y^2}$.

In the lossless case, r diverges when

$$k_y=k_{SP}\equiv(\omega/c)\sqrt{\frac{\epsilon_m\epsilon_d}{\epsilon_m+\epsilon_d}}, \tag{6}$$

where k_{SP} is the wave vector of the propagating surface polariton wave at the interface. As an example, at $\omega=1.785\times10^{14}$ rad/s ($\lambda=10.56$ μm, $\epsilon_m=-1.035$) [16] for the SiC–air interface, the transfer function indeed diverges at $k_{SP}=5.4k_d$ and decreases significantly above k_{SP}, setting a sharp cutoff in the wave-vector space for the transfer function [Fig. 2(b)].

In the realistic lossy material case, the wave has a maximum parallel wavevector at a frequency $\omega=1.785\times10^{14}$ rad/s [Fig. 2(a)]. For our purpose, therefore, we choose this frequency to be the operating frequency, which has $\epsilon_m=-1.035+0.13i$. The transfer function is shown in Fig. 2(c). It exhibits a maximum in the vicinity of the real part of $k_{SP}=2.3k_d$. Because the transfer function in the lossy case lacks the sharp peak in the lossless case, the cutoff of the largest usable wave vector is a soft one and can be pushed significantly beyond k_{SP} if a small focal length d is used. For example, in Fig. 2(c), the transfer function is above 50% in the evanescent region for k_y up to $8k_d$.

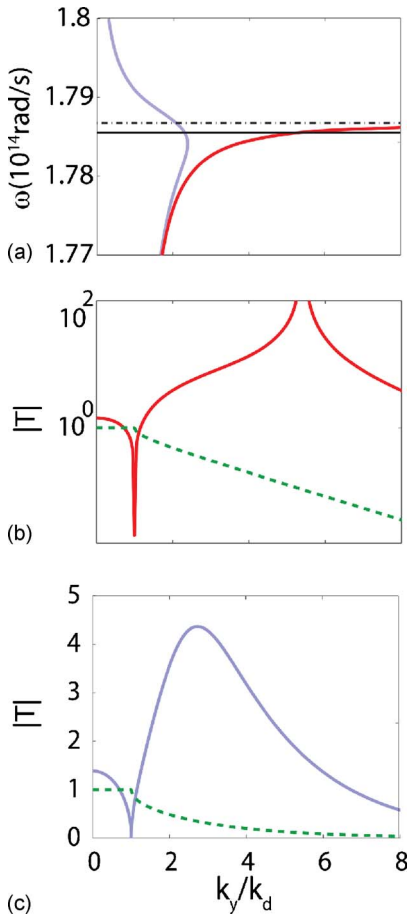

Fig. 2. (Color online) (a) Dispersion curve of k_{SP} at the interface between SiC and air. The black (blue)/gray (red) curves are calculated with or without the material loss, respectively. The dashed–dotted line shows the surface polariton frequency ω_{SP}, where real part of $\epsilon_m=-1$. The solid straight line shows the operating frequency used throughout the paper: $\omega=1.785\times10^{14}$ rad/s, $\lambda=10.56$ μm, $\epsilon_m=-1.035+0.13i$. (b) Absolute value of the amplitude transfer function with (solid curve) or without (dashed curve) the SiC. The SiC is assumed lossless with $\epsilon_m=-1.035$, $d=\lambda/15$. (c) Same as (b) but with material loss, $\epsilon_m=-1.035+0.13i$.

To demonstrate focusing at $z=d$, we find an initial field distribution by simply inverting the transfer function, so that we get a flat wave-vector spectrum at the image plane [5,15] [shown in Fig. 3(a)],

$$F_i(k_y,0)=\begin{cases}1/T(k_y), & -q_m<k_y<q_m\\ 0, & \text{otherwise}\end{cases}, \qquad (7)$$

where $q_m \equiv mk_d \gg k_d$ is the maximum spatial frequency that is proportional to the inverse of the size of the focal spot.

As a numerical demonstration, we consider the structure shown in Fig. 1(c). With an initial field $F_i(y,0)$ calculated from Eq. (7), using the transfer function in Fig. 2(c) and choosing $q_m=9k_d$, we get a focal spot with the FWHM=$\lambda/18$ at the focal plane $d=\lambda/15$ with peak amplitude gain [defined as $F(y=0,z=d)/F(y=0,z=0)$] of 3.0. [Fig. 1(d)]. Notice that, because the transfer function is relatively flat, the field shape does not evolve much. In contrast, a conventional radiationless focusing based on [5,8,9] with the same FWHM and focal length is shown in Figs. 1(a) and 1(b). The decay is clearly seen in the linear plot [Fig. 1(b)] where the peak amplitude decays to 7.8% at the focal plane. The structure in Figs. 1(c) and 1(d) uses k_y between $\pm 9k_d$. In contrast, the conventional scheme uses only evanescent components $5k_d<|k_y|<10k_d$.

In principle, the low Fourier wave-vector components, including the propagating ones, can also be used in a conventional scheme. However, without the evanescent amplification, the magnitude of the transfer function in the propagating region would be several orders of magnitude greater than that in the evanescent region. Therefore, small errors in the propagating wave at the incident field can dominate the rapidly decaying evanescent field at the image plane. As a result, a conventional scheme is restricted to using only the evanescent components. In our scheme, however, both propagating and evanescent regions can be used.

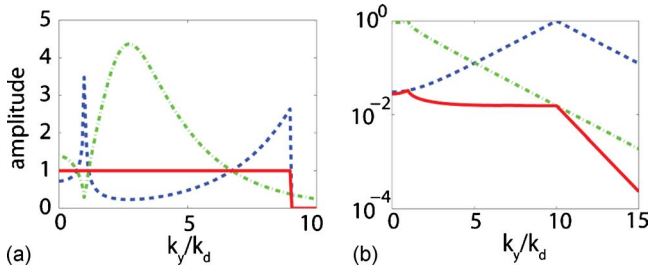

Fig. 3. (Color online) The green (dashed–dotted), blue (dashed), and red (solid) curves are the amplitude transfer function, the incident field amplitude spectrum, and the field amplitude spectrum at the focal point, respectively. (a) With evanescent amplification. (b) Without evanescent amplification.

For implementation of our scheme, a low-loss material is desirable. In the far IR, one can use SiC. In the visible wavelength range, one could potentially use the strong plasmonic response of metal; however, the loss of these materials is more severe than that of SiC in the far IR. In the near IR, one could consider the use of structured metal surface [17,18], which provides a surface state at a frequency controlled by geometry. In summary, our results overcome an important issue in a radiationless interference scheme by showing that evanescent decay needs not hamper subwavelength focusing.

Varat Intaraprasonk is supported by the Stanford Graduate Fellowships program.

References

1. J. B. Pendry, Phys. Rev. Lett. **85**, 3966 (2000).
2. N. Fang, H. Lee, C. Sun, and X. Zhang, Science **308**, 534 (2005).
3. D. Melville, R. Blaikie, and C. Wolf, Appl. Phys. Lett. **84**, 4403 (2004).
4. M. G. Silveirinha, C. A. Fernandes, and J. R. Costa, Phys. Rev. B **78**, 195121 (2008).
5. R. Merlin, Science **317**, 927 (2007).
6. L. E. Helseth, Opt. Commun. **281**, 1981 (2008).
7. L. E. Helseth, Phys. Rev. A **78**, 013819 (2008).
8. A. Grbic and R. Merlin, IEEE Trans. Antennas Propag. **56**, 3159 (2008).
9. A. Grbic, L. Jiang, and R. Merlin, Science **320**, 511 (2008).
10. L. Markley, A. Wong, Y. Wang, and G. Eleftheriades, Phys. Rev. Lett. **101**, 113901 (2008).
11. G. V. Eleftheriades and A. M. H. Wong, IEEE Microw. Wirel. Compon. Lett. **18**, 236 (2008).
12. A. B. Evlyukhin and S. I. Bozhevolnyi, Opt. Express **16**, 17429 (2008).
13. R. Gordon, Phys. Rev. Lett. **102**, 207402 (2009).
14. M. F. Imani and A. Grbic, IEEE Antennas Wireless Propag. Lett. **8**, 421 (2009).
15. V. Intaraprasonk and S. Fan, Opt. Lett. **34**, 2967 (2009).
16. E. D. Palik, ed., *Handbook of Optical Constants of Solids* (Academic, 1985).
17. J. B. Pendry, L. Martin-Moreno, and F. J. Garcia-Vidal, Science **305**, 847 (2004).
18. J. T. Shen, P. B. Catrysse, and S. Fan, Phys. Rev. Lett. **94**, 197401 (2005).